Regulation of neonatal and adult mammalian heart regeneration by the miR-15 family

Enzo R. Porrello[a,b,1], Ahmed I. Mahmoud[c,1], Emma Simpson[a], Brett A. Johnson[a], David Grinsfelder[c], Diana Canseco[c], Pradeep P. Mammen[c], Beverly A. Rothermel[a,c], Eric N. Olson[a,2], and Hesham A. Sadek[c,2]

Departments of [a]Molecular Biology and [c]Internal Medicine, University of Texas Southwestern Medical Center, Dallas, TX 75390; and [b]School of Biomedical Sciences, University of Queensland, St Lucia, Queensland 4072, Australia

Edited* by J. G. Seidman, Harvard Medical School, Boston, MA, and approved November 15, 2012 (received for review May 24, 2012)

We recently identified a brief time period during postnatal development when the mammalian heart retains significant regenerative potential after amputation of the ventricular apex. However, one major unresolved question is whether the neonatal mouse heart can also regenerate in response to myocardial ischemia, the most common antecedent of heart failure in humans. Here, we induced ischemic myocardial infarction (MI) in 1-d-old mice and found that this results in extensive myocardial necrosis and systolic dysfunction. Remarkably, the neonatal heart mounted a robust regenerative response, through proliferation of preexisting cardiomyocytes, resulting in full functional recovery within 21 d. Moreover, we show that the miR-15 family of microRNAs modulates neonatal heart regeneration through inhibition of postnatal cardiomyocyte proliferation. Finally, we demonstrate that inhibition of the miR-15 family from an early postnatal age until adulthood increases myocyte proliferation in the adult heart and improves left ventricular systolic function after adult MI. We conclude that the neonatal mammalian heart can regenerate after myocardial infarction through proliferation of preexisting cardiomyocytes and that the miR-15 family contributes to postnatal loss of cardiac regenerative capacity.

cardiac regenerative window | cardiomyocyte cell cycle | posttranscriptional regulation

The inability of the adult mammalian heart to regenerate after injury poses a major barrier in cardiovascular medicine (1). Although limited myocyte turnover occurs in the adult mammalian heart throughout life and after myocardial infarction (MI) (2–4), myocyte replenishment after injury is insufficient to restore contractile function to the damaged heart. In the absence of meaningful regeneration, the adult mammalian heart undergoes a series of pathological remodeling events including replacement of necrotic myocardial tissue with fibrotic scar tissue and pathological hypertrophy of the remaining viable myocardium, which ultimately contribute to contractile demise of the heart and organ failure. In contrast, teleost fish can regenerate heart muscle throughout life after mechanical, genetic, and cryoinjury (5–7). Whether natural mechanisms of endogenous cardiac regeneration can be recapitulated in adult mammals is unclear and represents an important issue for regenerative medicine.

We recently discovered that the neonatal mammalian heart retains significant cardiac regenerative potential for a brief time after birth. Similar to adult zebrafish, the neonatal mouse heart is capable of mounting an endogenous regenerative response after surgical amputation of the ventricular apex (8). Cardiomyocyte proliferation appears to be the major cellular mechanism driving cardiac regeneration in neonatal mice (8) and adult zebrafish (9, 10). However, the relationship between postnatal cell cycle arrest and loss of cardiac regenerative capacity in mammals is likely complex and may involve transformations in a number of organ systems and cell types during this critical postnatal transitional period. Nevertheless, these findings suggest that the molecular and cellular mechanisms required for endogenous heart regeneration are silenced in mammals shortly after birth. Two unresolved questions that are of fundamental importance to our understanding of mammalian heart regeneration are whether the neonatal heart can also regenerate after ischemic myocardial necrosis, which is the most pathophysiologically relevant form of cardiac injury, and whether the molecular mechanisms that regulate cardiac regenerative capacity in mammals can be identified and manipulated to extend the neonatal "cardiac regenerative window" into adulthood.

The molecular mechanisms that regulate cardiomyocyte proliferation and cardiac regenerative capacity in the neonatal period are poorly understood. MicroRNAs have recently emerged as important modulators of gene networks and often form intricate regulatory circuits together with transcription factors and histone modifiers to influence the expression of large numbers of genes in a biological pathway (11). We have shown that multiple members of a large microRNA family, known as the miR-15 family, are upregulated in the mouse heart shortly after birth and contribute to the repression of a number of cell cycle genes and postnatal cell cycle arrest (12). Whether the miR-15 family also plays a role in repressing cardiac regenerative capacity in mammals after birth has not been examined.

The goal of this study was to determine whether the neonatal mouse heart is capable of mounting an endogenous cardiac regenerative response to myocardial ischemia and whether the miR-15 family plays an active role in regulating cardiac regenerative capacity in neonatal mice. Here, we report that the neonatal mouse heart harbors a robust intrinsic capacity for cardiac regeneration after MI. Using both gain- and loss-of-function approaches, we demonstrate that the miR-15 family plays an important role in regulating cardiac regenerative capacity in mammals.

Results

Neonatal Heart Regenerates After MI. To establish how the neonatal mouse heart responds to ischemic injury, we permanently ligated the left anterior descending (LAD) coronary artery of 1-d-old mice (Fig. 1*A*). Evidence of myocardial necrosis was noted at day 3 after LAD ligation, where staining with the viability indicator triphenyltetrazolium chloride (TTC) revealed that the majority of the myocardium below the ligature (~75%) was nonviable (Fig. 1 *B* and *C*). LAD ligation was accompanied by a marked decline in left ventricular systolic function at 4 d after injury (Fig. 1*D*). Histological analysis confirmed that extensive cardiomyocyte loss and intramyocardial hemorrhaging had occurred after LAD ligation (Fig. 1*E*).

To assess the regenerative capacity of the neonatal mouse heart after ischemic injury, histological and functional analyses were performed at multiple time points after LAD ligation. Serial

Author contributions: E.R.P., A.I.M., E.N.O., and H.A.S. designed research; E.R.P., A.I.M., E.S., B.A.J., D.G., D.C., and H.A.S. performed research; P.P.M., B.A.R., and H.A.S. contributed new reagents/analytic tools; H.A.S. analyzed data; and E.R.P., A.I.M., E.N.O., and H.A.S. wrote the paper.

Conflict of interest statement: E.N.O. is a cofounder of miRagen Therapeutics, a company focused on developing miRNA-based therapies for cardiovascular disease.

*This Direct Submission article had a prearranged editor.

[1]E.R.P. and A.I.M. contributed equally to this work.

[2]To whom correspondence may be addressed. E-mail: eric.olson@utsouthwestern.edu or hesham.sadek@utsouthwestern.edu.

This article contains supporting information online at www.pnas.org/lookup/suppl/doi:10.1073/pnas.1208863110/-/DCSupplemental.

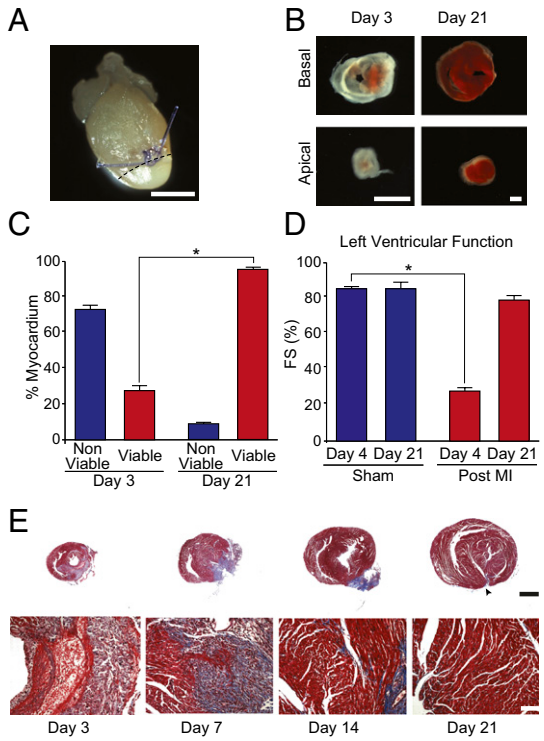

Fig. 1. Neonatal heart regeneration after MI. (*A*) Whole-mount image of a neonatal heart 1 day after LAD ligation at P1. Note blanching of the territory supplied by the LAD (area below dashed line). (*B*) TTC staining below the ligature at day 3 and 21 after LAD ligation. Basal and apical sections are shown for each heart. Red staining indicates viable myocardium. (*C*) Quantification of TTC staining at day 3 and 21 after LAD ligation demonstrating recovery of myocardial viability by day 21 after injury. Quantification represents analysis of a total of ~30 sections from four to five independent samples per group. (*D*) Left ventricular systolic function quantified by fractional shortening (FS) showing significant systolic dysfunction 4 d after MI, with restoration of normal systolic function by 21 d after MI. Values presented as means ± SEM; $n = 3$–5 per group; $^*P < 0.05$. (*E*) Low magnification (*Upper*) and high magnification (*Lower*) Masson's trichrome staining at multiple timepoints after MI. Note the extensive myocyte loss and inflammatory cell infiltration at 3 d after MI, followed by extracellular matrix deposition, then gradual restoration of normal anterior wall thickness by 21 d. There was little evidence of fibrosis at 21 d after MI, with the exception of a small region of fibrotic tissue at the site of the permanent ligature (arrowhead). (Scale bars: *A*, *B*, and *E*, 1 mm.)

histological analysis revealed progressive regeneration of the anterior wall of the infarcted neonatal heart over a period of 21 d (Fig. 1*E*). Masson's trichrome staining showed the accumulation of fibrotic tissue at 7 d after injury, which decreased by 14 d after injury (Fig. 1*E*). By 21 d after MI, there was little evidence of fibrosis, with the exception of a small region of fibrotic tissue at the site of the permanent ligature. We believe that this small area of resistance to regeneration is secondary to the persistence of the anatomical barrier represented by the ligature (Fig. 1*E*). Moreover, at 21 d after MI, greater than 95% of the myocardium was viable (Fig. 1 *B* and *C*) and cardiac systolic function was restored to sham-operated levels (Fig. 1*D*). Importantly, no signs of systolic dysfunction were apparent up to 9 mo after LAD ligation in 1-d-old mice (Fig. S1 *A* and *B*). These results are similar to those reported after cryocauterization in zebrafish, which is also associated with early scarring and the subsequent clearance of fibrotic tissue (7).

Post-MI Neovascularization. An important aspect of cardiac regeneration after coronary artery occlusion is the reestablishment of adequate blood flow to the infarcted myocardium. Coronary corrosion casts were performed at 7 and 21 d after LAD ligation of 1-d-old mice. Right-to-left and left-to-left collateral vessels were noted distal to the LAD ligature (Fig. S2 *A* and *B*) at 7 d but did not appear to anastomose with the ligated vessel until 21 d after ligation (Fig. S2 *C* and *D*). In addition, BrdU-positive large coronary vessels were noted in the infarct zone (Fig. S2*E*). These results indicate that neonatal heart regeneration is associated with a vascular response that restores perfusion to the infarcted myocardium.

Neonatal MI Induces Cardiomyocyte Proliferation. Heart regeneration in neonatal mice after ischemic injury was associated with robust and widespread induction of cardiomyocyte proliferation and sarcomere disassembly (Fig. 2). Induction of cardiomyocyte mitosis and cytokinesis were assessed by colocalization of phosphohistone H3 (pH3) and aurora B kinase, respectively, with cardiac troponin T. A significantly higher number of cardiomyocytes with disassembled sarcomeres (Fig. 2 *D* and *H*–*J*), and a significantly increased number of pH3-positive (Fig. 2 *C* and *G*) and aurora B-positive (Fig. 2 *E* and *F*) cardiomyocytes were identified in mice at day 7 after MI compared with sham-operated controls. Approximately 3–5% of cardiomyocytes were undergoing mitosis at day 7 after MI. Notably, proliferating cardiomyocytes were not restricted to the ischemic and border zones of the infarct but were also identified in the remote zone (i.e., posterior and lateral walls) (Fig. 2 *B*–*D* and *F*). Furthermore, pulse-chase labeling with BrdU (administered at days 1, 7, and 14) identified many BrdU-positive cardiomyocytes in the newly formed myocardium at day 21 after MI (Fig. 3 *A*–*C*). The number of BrdU-positive cardiomyocyte nuclei was augmented in the ischemic, border, and remote zones of the myocardium at day 21 after MI, indicating that many cardiomyocytes within the newly formed myocardium had undergone at least one round of DNA replication during the course of post-MI regeneration.

Newly Formed Cardiomyocytes Are Derived from Preexisting Cardiomyocytes. To establish the lineage of origin of regenerated cardiomyocytes, *Rosa26*-lacZ reporter mice were crossed with *Myh6*-MerCreMer mice, which harbor a tamoxifen-inducible Cre recombinase transgene under control of *Myh6* cardiomyocyte-specific promoter. Neonates were then given a single s.c. dose of tamoxifen at birth to label the preexisting cardiomyocyte population before LAD ligation (Fig. 3*D*), as described (8). Administration of a single dose of tamoxifen at birth resulted in ~70% of the myocardium being labeled with lacZ in the sham-operated group (Fig. 3*E*). Histological sections were acquired from sham and infarcted hearts at day 21 after MI. The majority of the newly formed myocardium stained positive for lacZ, with no differences in the percentage of lacZ-positive myocardium between sham and infarcted hearts in the ischemic, border, and remote zones (Fig. 3*E*). These findings provide genetic evidence that the majority of newly formed cardiomyocytes after MI in 1-d-old mice are derived from preexisting cardiomyocytes, rather than from a stem cell population.

Lack of Regeneration of 7- and 14-d-Old Infarcted Hearts. To determine whether the cardiac regenerative response to ischemic injury is lost when neonatal mouse cardiomyocytes withdraw from the cell cycle, we performed LAD ligation on 7- and 14-d-old mice. In contrast to 1-d-old mice, 7- and 14-d-old mice failed to regenerate after LAD ligation (Fig. 4 *A* and *B*). Whereas 1-d-old mice were capable of clearing fibrotic tissue and replenishing cardiomyocytes (Fig. 1*E*), 7-d-old mice retained significant scar tissue at day 21 after MI (Fig. 4*A*) and the cardiac remodeling response of 14-d-old mice after MI was similar to that of adult mice and was characterized by extensive fibrosis, wall thinning, and ventricular dilation (Fig. 4*B*). Very few proliferating cardiomyocytes with disassembled sarcomeres were identified after MI in 7-d-old mice (Fig. 4 *C* and *D*). In contrast to the regenerative response of the 1-d-old mouse heart, which occurred in the absence of any appreciable hypertrophic remodeling, cardiac repair in 14-d-old mice occurred coincident with cardiac and cardiomyocyte hypertrophy (Fig. 4 *E*–*G*),

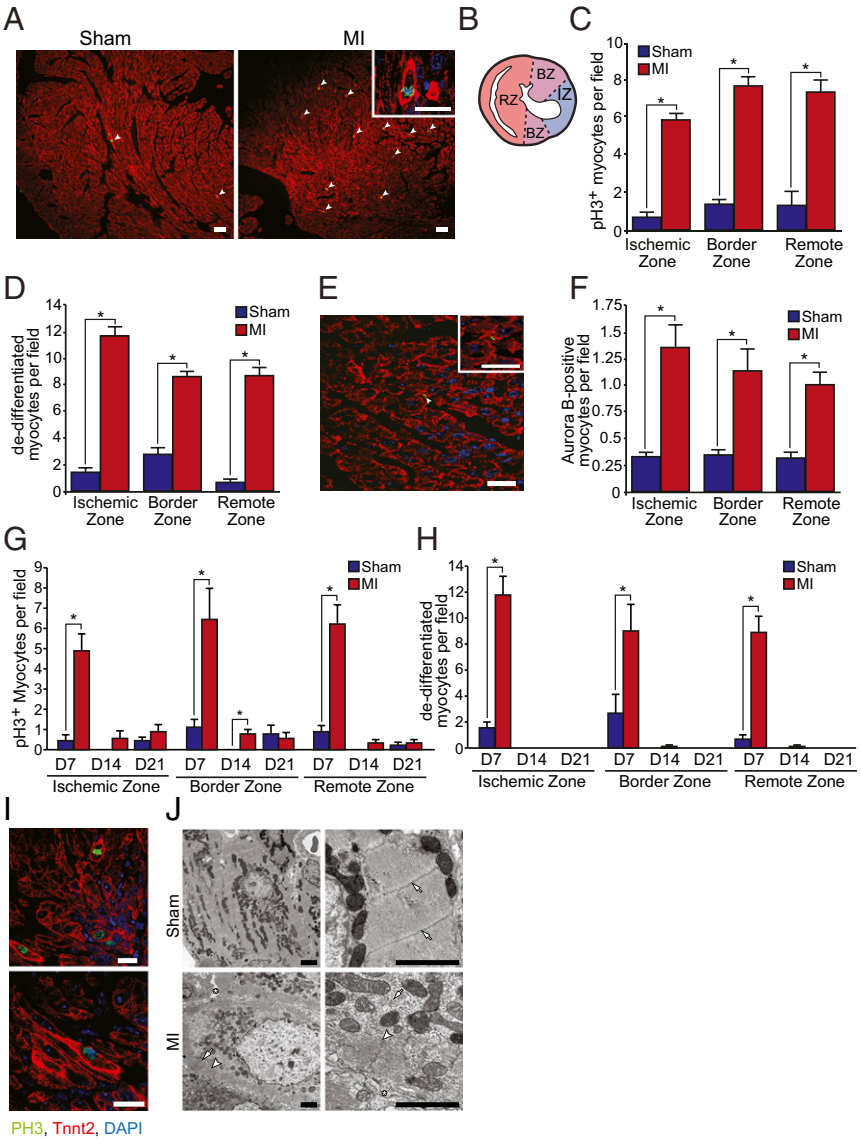

Fig. 2. Neonatal MI induces cardiomyocyte proliferation and dedifferentiation. (*A*) pH3 and troponin T staining of sham-operated and MI hearts at day 7 after surgery. Note the marked increase in pH3$^+$ cardiomyocytes with disassembled sarcomeres (arrowheads). *Inset* shows a higher magnification view of a pH3$^+$ cardiomyocyte with disorganized sarcomeric structure and intense troponin T staining around the periphery of the cell. (*B*) Cartoon depicting a transverse heart section after MI with ischemic, border, and remote zones used for quantification highlighted. (*C* and *D*) Quantification of the number of pH3$^+$ cardiomyocytes and cardiomyocytes with disassembled sarcomeres at 7 d after MI. (*E*) Aurora B staining of a cardiomyocyte undergoing cytokinesis at day 7 after MI. (*F*) Quantification of the number of aurora B$^+$ cardiomyocytes at 7 d after MI. (*G*) Quantification of cardiomyocyte mitosis in the ischemic, border, and remote zones of sham-operated and infarcted hearts at days 7, 14, and 21 after surgery. (*H*) Quantification of cardiomyocyte sarcomere disassembly in the ischemic, border, and remote zones of sham-operated and infarcted hearts at days 7, 14, and 21 after surgery. Quantitative analyses represent counting of multiple fields from three independent samples per group at each time point (~9 fields per region per time point). Values presented as mean ± SEM; *$P < 0.05$. (*I*) High resolution confocal microscopy images showing cardiomyocytes staining positive for pH3 (green) and troponin T (red) at day 7 after MI. Images are shown at low (*Upper*) and high (*Lower*) magnification. Note the complete disorganization of sarcomeric structure in pH3$^+$ cardiomyocytes and the marginalization of sarcomeres to the periphery of mitotic cardiomyocytes. (*J*) EM of sections of sham-operated (*Upper*) and infarcted hearts (*Lower*) at day 7 after surgery. Cardiomyocytes in sham-operated control samples show a tightly organized sarcomeric structure and Z-lines are clearly visible at higher magnification (arrows). In contrast, regenerating cardiomyocytes in MI hearts have a disorganized sarcomeric structure (arrows), along with the appearance of intercellular spaces (asterisk) and also contained sarcomeres aligned along the periphery of the cardiomyocyte (arrowheads). (Scale bars: *A*, 50 μm; *A Inset*, *E*, and *I*, 20 μm; *J*, 2 μm.)

which is a hallmark feature of pathological remodeling in the adult heart. These results indicate that cardiac regenerative capacity in mice is lost by 1 wk of postnatal life.

miR-195 Transgenic Hearts Fail To Regenerate After MI. The molecular mechanisms regulating cardiac regenerative capacity after birth in mammals are unknown. We recently discovered that multiple members of the miR-15 family of microRNAs are up-regulated in the mouse heart shortly after birth and contribute to cardiomyocyte mitotic arrest (12). Consistent with their inhibitory effect on myocyte proliferation, we found that several members of the miR-15 family were down-regulated at 3 d after MI at P1 (Fig. S3*A*). Importantly, miR-15 family members were down-regulated in infarcted myocardium (below the LAD ligature), and in noninfarcted myocardium (above the ligature), suggesting that these differences were not a consequence of myocyte loss in the infarct zone. To test whether the miR-15 family regulates cardiac regenerative capacity in neonatal mice, miR-195 (a member of the miR-15 family) was overexpressed in the developing heart (12). MYH7-miR-195 transgenic (TG) mice underwent LAD ligation at P1. We reported that a small subset (~22%) of these TG mice have preexisting ventricular septal defects at birth (12). These mice were identified after MI by histological analysis and by dilation of the right ventricle and cardiac wall motion abnormalities upon echocardiography. TG mice with preexisting VSDs were excluded from subsequent analyses. TG mice that did not have preexisting VSDs had normal baseline cardiac function at 3 wk of age (Fig. 5*C*). At day 7 after MI, MYH7-miR-195 TG mouse hearts showed fewer proliferating cardiomyocytes (Fig. 5 *A* and *B* and Fig. S3*B*), more proliferating nonmyocytes (Fig. S3*C*), and hypertrophic cardiomyocytes (Fig. 5 *E* and *F*). Echocardiography showed that MYH7-miR-195 TG mice had significantly depressed contractile function at day 21 after MI compared with wild-type mice (Fig. 5*C*). Moreover, histological assessment of the MYH7-miR-195 TG hearts 21 d after MI showed extensive anterior wall fibrosis extending to the apex and defective regeneration (Fig. 5*D*). Microarray analyses on injured WT and miR-195 TG mice indicated that miR-195 overexpression in cardiomyocytes was associated with the modest repression of a number of cell cycle and mitochondrial genes, and the induction of many inflammatory genes after MI (Fig. S4). These findings demonstrate that miR-195 overexpression in cardiomyocytes is sufficient to impair the regenerative response of the 1-d-old mouse heart resulting in adult-like remodeling after MI.

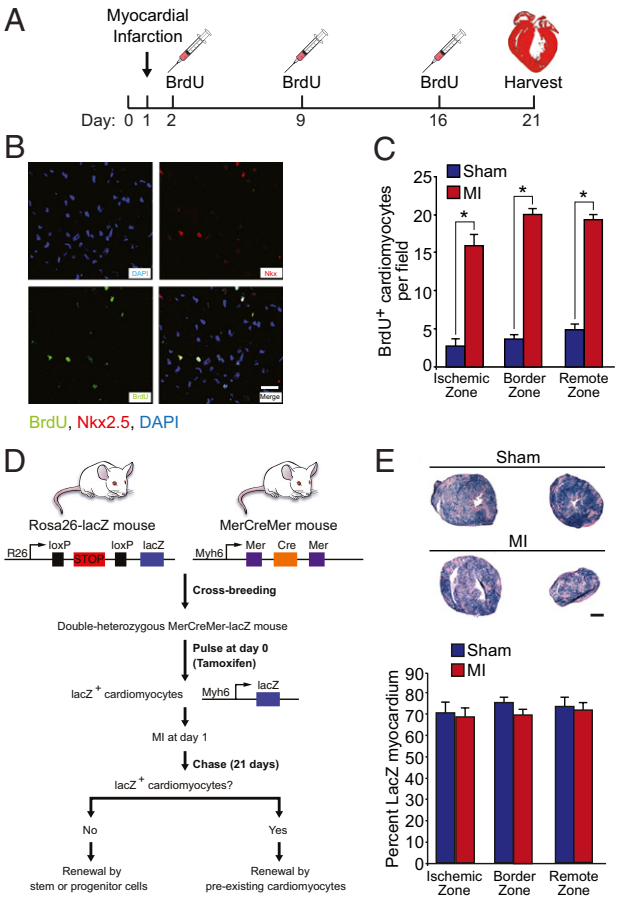

Fig. 3. Determining the lineage origin of newly formed cardiomyocytes. (*A*) Schematic of BrdU administration protocol. (*B*) Immunostaining showing colocalization of BrdU and Nkx2.5 at day 21 after MI. (Scale bar: 20 μm.) (*C*) Quantification of the number of $BrdU^+/Nkx2.5^+$ nuclei at day 21 after MI. Quantitative analysis represents counting of multiple fields from three independent samples per group (~9 fields per region). (*D*) Schematic of cardiomyocyte lineage tracing study design. (*E Upper*) β-galactosidase enzymatic staining of MYH6-MerCreMer; Rosa26-lacZ reporter mouse heart showing similar staining in sham and MI hearts at day 21 after surgery. Basal and apical sections (below ligature) are shown for each heart. (*E Lower*) Quantification of the percentage of $lacZ^+$ myocardium in sham and MI hearts showing no difference across regions of the heart. Quantitative analysis represents counting of multiple fields from three independent samples per group (~9 fields per region). Values presented as mean ± SEM; $*P < 0.05$.

Inhibition of the miR-15 Family Increases Adult Myocyte Proliferation and Improves Cardiac Function After Adult MI. To determine whether postnatal inhibition of the miR-15 family can induce adult myocyte proliferation, we administered locked nucleic acid (LNA)-modified anti-miRs to neonatal mice by s.c. injection at postnatal days (P)1, 7, and 14 to inhibit the expression of the miR-15 family until adulthood (Fig. 6*A* and Fig. S5*A*). At P21, MI was induced by using an LAD ligation/reperfusion model. Given that the effects of inhibition of the miR-15 family on the coronary vasculature are uncharacterized, we used an ischemia-reperfusion model rather than permanent LAD ligation to better control the effects of the anti-miR treatment on the myocyte compartment. We found that inhibition of the miR-15 family was associated with similar infarct size between the two groups (Fig. 6 *B*–*D*). Moreover, inhibition of the miR-15 family from birth until adulthood resulted in induction of myocyte proliferation in the infarcted adult heart and a gradual improvement in left ventricular systolic function after MI over time (Fig. 6 *E* and *F* and Fig. S5 *B* and *C*), indicating that postnatal inhibition of the miR-15 family promoted myocardial regeneration. Because of the lack of cardiomyocyte specificity of the anti-miR administration protocol, inhibition of the miR-15 family was also associated with the robust induction of proliferation in the nonmyocyte compartment after MI (Fig. S5*D*), but the significance and therapeutic relevance of these non-cardiomyocyte effects are unclear. These findings suggest that postnatal inhibition of the miR-15 family prevents cardiomyocyte cell cycle arrest in a subset of cardiomyocytes and improves cardiac function after MI.

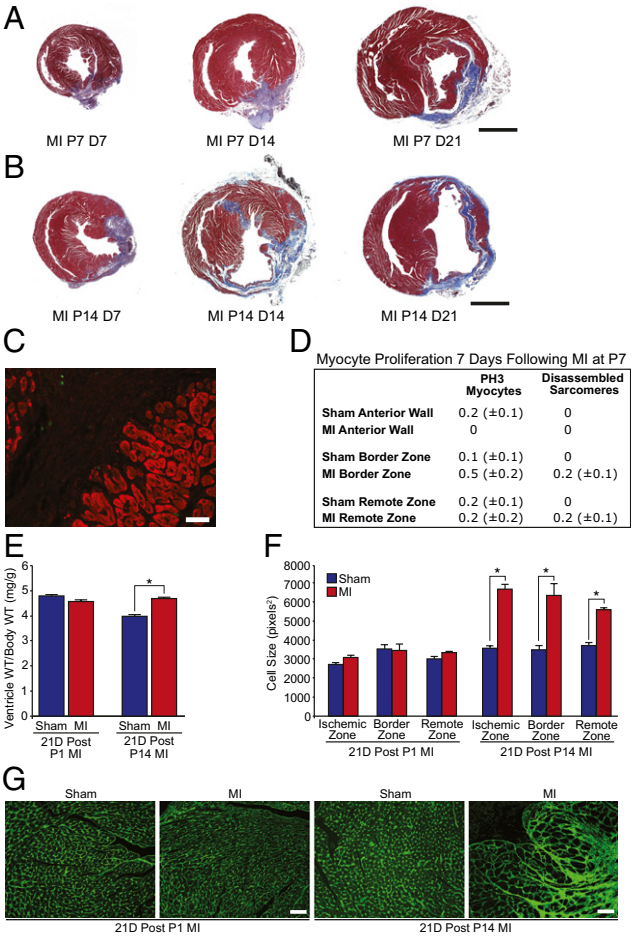

Fig. 4. Lack of regeneration of 7- and 14-d-old hearts after MI. (*A*) Masson's trichrome staining of hearts infarcted at P7 showing fibrosis and lack of regeneration at 7, 14, and 21 d after MI. (*B*) Masson's trichrome staining of hearts infarcted at P14 showing a lack of regeneration and significant pathological remodeling at 7, 14, and 21 d after MI. (*C* and *D*) Immunostaining and quantification of $pH3^+$ cardiomyocytes and cardiomyocytes with disassembled sarcomeres at day 7 after MI showing lack of myocyte proliferation after MI at P7. Quantitative analyses represent counting of multiple fields from three independent samples per group (~9 fields per region). Values presented as mean ± SEM. (*E*) Ventricle weight to body weight ratios for sham and MI groups at 21 d after surgery at either P1 or P14. Values presented as mean ± SEM; $n = 5$ per group; $*P < 0.05$. (*F*) Cell size quantification showing no change in cell size at day 21 after MI at P1 and significant myocyte hypertrophy in the ischemic, border, and remote zones at day 21 after MI at P14. (*G*) Wheat germ agglutinin staining for sham and MI groups at 21 d after surgery at either P1 or P14. Quantitative analyses represent counting of multiple fields from three independent samples per group (~90 cells assessed per heart). Values presented as mean ± SEM; $*P < 0.05$. (Scale bars: *A* and *B*, 1 mm; *C*, 20 μm; *G*, 50 μm.)

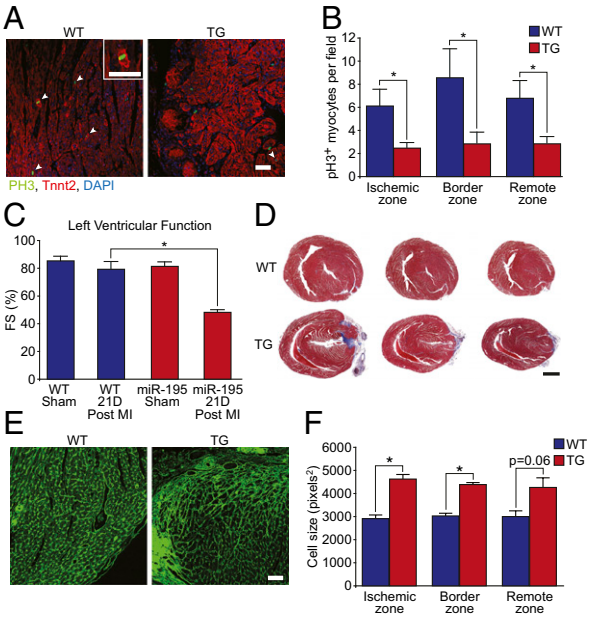

Fig. 5. miR-195 overexpression inhibits neonatal heart regeneration. (*A*) Immunostaining of WT and TG hearts showing a markedly decreased number of pH3$^+$ cardiomyocytes at day 7 after MI in TG hearts. Arrowheads denote pH3+ cardiomyocytes. *Inset* is a high magnification image of a cardiomyocyte with disassembled sarcomeres positively stained for pH3. (*B*) Quantification of pH3$^+$ cardiomyocytes in WT and TG hearts at day 7 after MI. Quantitative analysis represents counting of multiple fields from three independent WT and four TG samples per group (~9 fields per region). Values presented as mean ± SEM; $*P < 0.05$. (*C*) Left ventricular systolic function quantified by FS in WT and TG mice at baseline and at 21 d after MI at P1. Values presented as mean± SEM; $n = 5–8$ samples per group; $*P < 0.05$. (*D*) Masson's trichrome stained sections showing fibrosis and lack of regeneration of TG hearts at day 21 after MI. (*E*) Wheat germ agglutinin staining of WT and TG hearts at day 21 after MI at P1. (*F*) Quantification of cell size showing significant myocyte hypertrophy in the ischemic, border, and remote zones at day 21 after MI in miR-195Tg hearts. Quantitative analyses represent counting of multiple fields from three independent samples per group (~90 cells assessed per heart). Values presented as mean ± SEM; $*P < 0.05$. (Scale bars: *A* and *E*, 50 μm; *D*, 2 mm.)

Conclusions

Although the majority of mammalian cardiomyocytes undergo cell cycle arrest shortly after birth, modest, but measurable, cardiomyocyte turnover occurs in adult mouse and human hearts (2, 3, 13–17). However, this myocyte turnover is insufficient for restoration of cardiac contractile function after injury. In contrast to the adult mammalian heart, the neonatal mouse heart has significant regenerative potential for the first few days of life. Our findings indicate that the neonatal mouse heart is capable of mounting a robust regenerative response after ischemic myocardial necrosis, which is mediated primarily through proliferation of preexisting cardiomyocytes.

In our genetic labeling studies of cardiomyocytes, only 70% of cardiomyocytes were labeled by lacZ expression, raising the possibility that 30% of unlabeled cardiomyocytes are derived from an unidentified stem or progenitor population. However, no fate mapping studies have been performed to date to examine this possibility. Although a recent report showed activation of a c-kit reporter after myocardial cryoinjury in the neonate (18), it is difficult to reach a conclusion about some minor role of progenitor cells in neonatal heart regeneration without carefully designed fate mapping studies. Although c-kit is expressed in a subset of cardiac progenitor cells, it is known that c-kit is also expressed during cardiomyocyte dedifferentiation (19, 20), and proliferation (21), which are known features of the neonatal cardiac regenerative response. Therefore, future studies using detailed analysis of the extent and mechanism of regeneration in the neonatal cryoinjury model are warranted.

Although a full understanding of the mechanism of neonatal heart regeneration remains elusive, the current report highlights a role of the miR-15 family in this process. Using both gain- and loss-of-function genetic and pharmacological approaches in the neonatal cardiac injury model, we have found that the miR-15 family, which inhibits cardiomyocyte proliferation and represses a number of cell cycle genes in the heart, modulates neonatal heart regeneration. These results suggest that postnatal up-regulation of the miR-15 family may be an important regulatory component of a molecular pathway that arrests cardiomyocyte proliferation and cardiac regenerative capacity after birth. However, there are several limitations to the transgenic and anti-miR experiments reported in our study that warrant further discussion and that will require future follow-up studies. For instance, a subset (~22%) of MYH7-miR-195 transgenic mice are born with preexisting congenital heart abnormalities (12). These mice were excluded from our functional analyses and endpoints. The MYH7 transgene is activated during early embryonic cardiac development, and although cardiac function is normal in the majority of MYH7-miR-195 transgenic mice prior to injury, we cannot completely exclude a potential contribution of an underlying subtle pathology in these mice to the impaired regenerative phenotype after MI. Future studies using inducible transgenic mice or other technologies that allow for more precise temporal control of microRNA expression in vivo may help to resolve this question.

Members of the miR-15 family, like other microRNAs, engage a broad collection of mRNA targets including numerous cell cycle regulatory proteins and survival factors to exert their functions (22). Thus, the potential suppression of the regenerative response by the miR-15 family likely involves actions of numerous protein targets. Although the current study design points to a developmental contribution of the miR-15 family to regenerative arrest in the neonatal period, acute inhibition of this microRNA family after MI is obviously a more therapeutically relevant experimental paradigm. In this regard, acute inhibition of the miR-15 family in adult mice is associated with improved contractile function after ischemia-reperfusion injury (22).

The current findings in neonatal mice suggest that therapeutic strategies aimed at restoring the proliferative potential of adult mammalian cardiomyocytes will be an important component of attempts to reactivate the dormant regenerative capacity of the adult mammalian heart after MI. The neonatal mouse model represents a useful tool for modulation of mammalian cardiac regeneration and for understanding the complex cellular and molecular mechanisms that govern cardiomyocyte proliferative capacity.

Methods

Experimental Animals. All protocols were approved by the Institutional Animal Care and Use Committee of the University of Texas Southwestern Medical Center. Timed-pregnant ICR/CD-1 mice (Charles River Laboratories) were used to deliver pups for neonatal surgical procedures. MYH7-miR-195 transgenic mice were maintained on a mixed genetic background (12) and were bred to female ICR/CD-1 mice to deliver pups for neonatal surgeries.

Neonatal MI. MI surgeries were performed on neonatal mice (ICR/CD-1 strain; Charles River Laboratories) at P1 and P7. Neonates were anesthetized by cooling on an ice bed, as described (8). Lateral thoracotomy at the fourth intercostal space was performed by blunt dissection of the intercostal muscles after skin incision. A tapered needle (C-1) attached to a 6-0 prolene suture (Ethicon) was passed through the midventricle below the origin of the LAD coronary artery and tied to induce infarction. The pericardial membrane remained intact after LAD ligation. Myocardial ischemia was indicated by the light pallor of the myocardium below the ligature after suturing. After LAD ligation, neonates were removed from the ice bed, thoracic wall incisions were sutured with a 6-0 nonabsorbable prolene suture, and the skin wound closed by using skin adhesive. Sham-operated mice underwent the same procedure involving hypothermic anesthesia and thoracotomy without LAD ligation. No differences in the myocyte proliferative response were observed

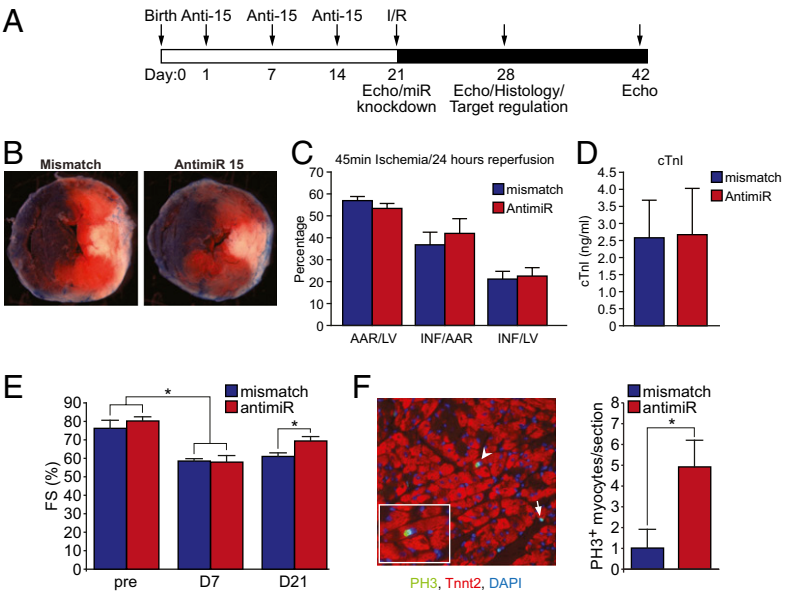

Fig. 6. Postnatal inhibition of the miR-15 family induces cardiomyocyte proliferation and improves cardiac function after MI. (*A*) Schematic of anti-miR (Anti-15) administration and I/R injury timeline. (*B*) Representative images of mismatch- and anti-miR–treated hearts after 45 min of ischemia and 24 h of reperfusion. Hearts were perfused with Evans blue dye, and sections were stained with the redox indicator TTC to quantify the extent of myocardial injury. Blue staining represents unaffected, remote myocardium; red staining indicates the area at risk (AAR); white myocardium represents the infarct area of necrosis. (*C*) Quantification of infarct size in mismatch- and anti-miR–treated mice at 24 h after I/R. The final infarct size is represented as the percentage of AAR/total area of left ventricle (LV), area of infarct (INF)/AAR, and INF/LV. Quantitative analyses represent counting from five mismatch and four anti-miR samples per group (~4–6 sections per sample). Values presented as mean ± SEM. (*D*) Serum levels of cardiac troponin I (cTnI) in mismatch- and anti-miR–treated mice at 24 h after I/R. Values presented as mean ± SEM; $n = 4$ per group. (*E*) Left ventricular systolic function quantified by fractional shortening (FS) in mismatch and anti-miR–treated mice at baseline and at 7 and 21 d after I/R. Values presented as mean ± SEM; $n = 4$ (mismatch) and $n = 5$ (anti-miR); $^*P < 0.05$. (*F Left*) Image showing proliferating pH3$^+$ cardiomyocytes (arrowheads) and proliferating non-myocyte (arrow) in anti-miR–treated heart. *Inset* is a high magnification image of a cardiomyocyte positively stained for pH3. (*F Right*) Quantification of pH3$^+$ cardiomyocytes in mismatch and anti-miR–treated hearts at day 7 after I/R. Quantitative analysis represents counting of 5–7 sections from five independent samples per group. Values presented as mean ± SEM; $^*P < 0.05$.

between sham-operated mice (hypothermic anesthesia and thoracotomy) and unoperated control mice. After surgery, neonates were warmed for several minutes under a heating lamp until recovery. The entire procedure lasted ~10 min. Ninety percent of sham-operated and LAD-ligated P1 and P7 neonates survived the surgical procedure, with all deaths occurring during or on the day of surgery. However, maternal cannibalization reduced survival rates in the MI group the following day to ~70%. For MI surgeries at P14, mice were anesthetized with isoflurane, followed by endotracheal intubation for ventilation by using a small animal ventilator (Harvard Apparatus).

Adult MI. Ischemia/reperfusion (I/R) surgeries were performed on 3-wk-old mice. After isofluorane anesthesia, the mice underwent endotracheal intubation and mechanical ventilation, followed by thoracotomy and I/R (45 min of ischemia induced by LAD ligation). The chest was closed, and the animals were extubated after recovery.

Genetic Fate Mapping Study. We crossed cardiomyocyte-specific MerCreMer mice [Tg(Myh6-cre/Esr*)1Jmk/J; The Jackson Laboratory] with *Rosa26*-lacZ-flox–targeted mice (*Gtrosa26*^{tm1Sor}; The Jackson Laboratory) to generate a tamoxifen-inducible cardiomyocyte reporter strain for genetic fate mapping (23). Induction of Cre recombinase activity and lacZ reporter expression was achieved by administering a single 2-mg dose of tamoxifen (Sigma), dissolved in sesame oil (Sigma), s.c. to neonatal mice at birth, as described (8). The following day, neonates underwent LAD ligation. At 21 d after MI, hearts were harvested, embedded in tissue freezing medium and flash frozen in 2-methylbutane cooled on liquid nitrogen (Sigma). Cryosections (8 μm) of the myocardium below the ligature were stained with X-gal staining solution for 48 h at 37 °C to detect lacZ activity. Sections were counterstained with nuclear fast red, and the percentage of myocardial tissue stained positive for lacZ was quantified by using Image J software.

ACKNOWLEDGMENTS. We thank J. Richardson, J. Shelton, and the University of Texas Southwestern Histology Core for help with histopathology; C. Gilpin for assistance with electron microscopy; J. Cabrera for graphical assistance; and E. van Rooij and miRagen Therapeutics for providing the anti-miRs. This work was supported by a C. J. Martin Overseas Biomedical Fellowship from the National Health and Medical Research Council and National Heart Foundation of Australia, National Health and Medical Research Council of Australia Project Grant APP1033815 (to E.R.P.), a predoctoral fellowship award from the American Heart Association (AHA) (to A.I.M.), grants from the National Institutes of Health (NIH), the Donald W. Reynolds Center for Clinical Cardiovascular Research, the Leducq Foundation, and the Robert A. Welch Foundation (E.N.O.), a cardiovascular research scholar award from Gilead Sciences, an AHA Grant-in-Aid award (AHA12GRNT), and an NIH R01 Grant (1R01HL115275-01) (to H.A.S.).

1. Laflamme MA, Murry CE (2011) Heart regeneration. *Nature* 473(7347):326–335.
2. Bergmann O, et al. (2009) Evidence for cardiomyocyte renewal in humans. *Science* 324(5923):98–102.
3. Hsieh PC, et al. (2007) Evidence from a genetic fate-mapping study that stem cells refresh adult mammalian cardiomyocytes after injury. *Nat Med* 13(8):970–974.
4. Kajstura J, et al. (2010) Cardiomyogenesis in the adult human heart. *Circ Res* 107(2):305–315.
5. Poss KD, Wilson LG, Keating MT (2002) Heart regeneration in zebrafish. *Science* 298 (5601):2188–2190.
6. Wang J, et al. (2011) The regenerative capacity of zebrafish reverses cardiac failure caused by genetic cardiomyocyte depletion. *Development* 138(16):3421–3430.
7. González-Rosa JM, Martín V, Peralta M, Torres M, Mercader N (2011) Extensive scar formation and regression during heart regeneration after cryoinjury in zebrafish. *Development* 138(9):1663–1674.
8. Porrello ER, et al. (2011) Transient regenerative potential of the neonatal mouse heart. *Science* 331(6020):1078–1080.
9. Kikuchi K, et al. (2010) Primary contribution to zebrafish heart regeneration by gata4(+) cardiomyocytes. *Nature* 464(7288):601–605.
10. Jopling C, et al. (2010) Zebrafish heart regeneration occurs by cardiomyocyte dedifferentiation and proliferation. *Nature* 464(7288):606–609.
11. Small EM, Olson EN (2011) Pervasive roles of microRNAs in cardiovascular biology. *Nature* 469(7330):336–342.
12. Porrello ER, et al. (2011) MiR-15 family regulates postnatal mitotic arrest of cardiomyocytes. *Circ Res* 109(6):670–679.
13. Beltrami AP, et al. (2001) Evidence that human cardiac myocytes divide after myocardial infarction. *N Engl J Med* 344(23):1750–1757.
14. Beltrami AP, et al. (2003) Adult cardiac stem cells are multipotent and support myocardial regeneration. *Cell* 114(6):763–776.
15. Orlic D, et al. (2001) Bone marrow cells regenerate infarcted myocardium. *Nature* 410(6829):701–705.
16. Soonpaa MH, Field LJ (1997) Assessment of cardiomyocyte DNA synthesis in normal and injured adult mouse hearts. *Am J Physiol* 272(1 Pt 2):H220–H226.
17. Li F, Wang X, Capasso JM, Gerdes AM (1996) Rapid transition of cardiac myocytes from hyperplasia to hypertrophy during postnatal development. *J Mol Cell Cardiol* 28(8):1737–1746.
18. Jesty SA, et al. (2012) c-kit+ precursors support postinfarction myogenesis in the neonatal, but not adult, heart. *Proc Natl Acad Sci USA* 109(33):13380–13385.
19. Zhang Y, et al. (2010) Dedifferentiation and proliferation of mammalian cardiomyocytes. *PLoS ONE* 5(9):e12559.
20. Kubin T, et al. (2011) Oncostatin M is a major mediator of cardiomyocyte dedifferentiation and remodeling. *Cell Stem Cell* 9(5):420–432.
21. Li M, et al. (2008) c-kit is required for cardiomyocyte terminal differentiation. *Circ Res* 102(6):677–685.
22. Hullinger TG, et al. (2012) Inhibition of miR-15 protects against cardiac ischemic injury. *Circ Res* 110(1):71–81.
23. Sohal DS, et al. (2001) Temporally regulated and tissue-specific gene manipulations in the adult and embryonic heart using a tamoxifen-inducible Cre protein. *Circ Res* 89(1):20–25.